Strong tumor MR contrast enhancement with novel nanomaterial in an oncogene-driven breast cancer model

Poster No.:	C-0212
Congress:	ECR 2014
Type:	Scientific Exhibit
Authors:	O. Axelsson, E. Aaltonen, R. Petoral Jr, P. Lauritzson, L. Hansson, P.-O. Eriksson; Lund/SE
Keywords:	Contrast agent-intravenous, MR, Oncology, Breast, Cancer
DOI:	10.1594/ecr2014/C-0212

Aims and objectives

Magnetic resonance imaging (MRI) has high spatial resolution, involves no ionizing radiation, and has therefore come to play a pivotal role for the visualization and quantification of tumors. The contrast agents (CA) used in many MRI investigations to improve the specificity and sensitivity of tumor diagnosis are small molecules containing gadolinium (Gd). The primary method in clinical practice is dynamic imaging [1]. This method requires fast acquisition which comes at the cost of spatial resolution, resulting in too many false-positives. As an example, according to Houssami et al., the positive predicted value was only 66 % in a meta-analysis of breast cancer MRI [2]. The time window for imaging is also very narrow with small molecule CAs. Furthermore, in 2004 it was found that some Gd-containing CAs could cause nephrogenic systemic fibrosis (NSF), a very serious side effect. This has lead to an increased interest in non-Gd based CAs [3].

The endothelial cells of capillaries of most tissues form a barrier which limits passage of macromolecules. On the other hand, tumor vasculature is leaky to large molecules. Additionally, tumors frequently lack lymphatic vessels. Collectively, these features lead to an effect termed enhanced permeability and retention (EPR) [4]. This effect can be exploited by choosing a nano-sized CA. The EPR effect causes nanoparticles with a suitable size to remain inside healthy vessels but selectively leak into tumor tissue, enabling a selective tumor contrast enhancement.

Considering the the above mentioned shortcomings, an obvious improvement would be a macromolecular, non-Gd based CA enabling high sensitivity to be combined with an increased spatial resolution and hence an improved specificity. It would be further beneficial if this would allow for an extended time window for imaging.

The aim of the current report was to test the potential of a new nanomaterial, SpagoPix, as a macromolecular MR contrast agent for tumor detection and to verify the presence of nanomaterial in tumor tissue. We demonstrate excellent tumor contrast enhancement with the new nanomaterial which consists of a polymeric, manganese-containing organo-phosphosilicon hydrogel with a PEG surface layer. Selective leakage into tumor tissue is demonstrated by chemical analysis and immunohistochemistry in a clinically relevant mouse model (MMTV-PyMT) of breast cancer.

Methods and materials

Animals: All animal experiments were approved by the Regional Ethical Committees for Animal Research at Stockholm or Lund, Sweden (ethical approvals ID; N96/11, N200/12 and N258/11). MMTV-PyMT mice for the imaging studies were bred and housed at

the Department of Medical Biochemistry and Biophysics, Division of Vascular Biology, Karolinska Institutet, Stockholm, Sweden (Kristian Pietras laboratory). NMRI mice and SD rats (Charles River Laboratories, Germany) were housed at Adlego Biomedical AB (Solna, Sweden). All animals were housed under standard animal facility conditions with free access to standard rodent chow and water.

Nanomaterial: The SpagoPix nanomaterial coated with m-PEG6-9-propyltrimethoxysilane was prepared according to example 10-11 in Axelsson et al. (patent WO2013041623A1)[5]. Material between 100 and 10 kDa was collected by laminar flow filtration. The nanomaterial was characterized by gel permeation chromatography (GPC), dynamic light scattering (DLS), zeta potential and relaxivity measurements. The size distribution and average hydrodynamic diameter were measured by GPC by comparing with protein standards of known size (bovine serum albumin and myoglobin). Hydrodynamic diameter and zeta-potential was measured by DLS on a Malvern Zetasizer Nano ZS equipped with a back-scattering detector (173°) 8 (Malvern Instruments Ltd, Malvern, England). For zeta potential measurements the parameters were 25 °C and 150 V. The longitudinal relaxivity (r_1) was measured using a Minispec mq60 NMR analyzer (60 MHz, Bruker Corporation, Billerica, MA) at 37 °C, and the samples were diluted in either MilliQ water or human blood plasma (Sigma Aldrich, St. Louis, MO).

Elemental analysis (ICP-AES): Elemental analysis was performed with an Optima 8300 instrument (PerkinElmer, Waltham, MA). Plasma samples were diluted in 0.1% HNO_3 prior to injection. Digested tumor and muscle samples were injected without dilution.

Pharmacokinetics and biodistribution: Three male SD rats were injected intravenously with a SpagoPix dose corresponding to 20 µmol Mn/kg. Blood samples were serially collected at 5, 20, 60 and 120 minutes and plasma concentrations of Mn and Si were analyzed by ICP-AES.

For the biodistribution studies, mice were euthanized after MR imaging. Tumors and femoral skeletal muscles were excised and prepared prepared for immunohistochemistry or digested in high concentration of HNO_3 for elemental analysis.

MRI: Two MR imaging studies were done with a clinical 3 T MR scanner using a human wrist coil. An overview of the scanning parameters is shown in Table 1. Anesthetized animals were intravenously injected with a SpagoPix dose corresponding to 20 µmol Mn/ kg. When imaged, the animals were immobilized in a modified 50 ml syringe on top of a 37 °C heating pad in the MR scanner.

Image analysis: MRI scan data were obtained as DICOM files and analyzed with OsiriX software (64-bit Open Source). For quantitative analysis, coronal imaging planes at as close as possible identical depths were identified for images at all imaging times for each individual animal. At each imaging plane, one region of interest (ROI) was placed in the upper black left quadrant outside the animal and defined as background. Depending on the availability of well-defined muscle tissue, one or two ROIs were placed separately on either fore- or hind limb muscle tissue. One ROI was placed on each tumor present in the determined image plane. Mean signal intensity and # (the background signal intensity standard deviation) was determined by the software for each ROI. The signal-to-noise ratio (SNR) was calculated by dividing the mean signal intensity by # and the tumor versus muscle contrast-to-noise ratio (CNR) was calculated by subtracting SNR_{muscle} from SNR_{tumor}. Images for visual presentation were treated with global automatic levels settings with GIMP (GNU Image Manipulation Program, version 2.8.2).

Immunohistochemistry: Paraformaldehyde fixed and paraffin embedded tumor and muscle tissues were cut and positioned on glass tissue slides. Deparaffinized sections were stained for PEG in an automated immunohistochemistry robot (Autostainer; Dako, Glostrup, Denmark) using a primary 0.6 µg/ml rabbit anti-PEG-B-47 antibody (Abcam, Cambride, MA) and a secondary goat-anti rabbit (1:200) antibody (Dako). The stained slides were digitized and total PEG-staining was quantified with Visomorph software (Visiopharm, Hoersholm, Denmark).

Statistical analysis: Differences between groups were analyzed with unpaired t-tests with the statistical package R (version 3.0.2). For MR CNR quantification, all tumors were treated separately and pooled data from the two studies were analyzed. Statistical significance was assumed at $p < 0.05$.

Images for this section:

Parameter	Study 1	Study 2
Scanning Sequence	SE	SE
Scan Options	SFS	SFS
MR Acquisition Type	2D	2D
Slice Thickness (mm)	2	2
Repetition Time (ms)	350	320
Echo Time (ms)	9.4	9.4
Number of Averages	2	11
Magnetic Field Strength (T)	3	3
Spacing Between Slices (mm)	2.2	2.2
Phase Encoding Steps	390/408	258
% Phase Field of View	79.69	100
Pixel Bandwidth	300	300
Acquisition Matrix	0\256\204\0	0\256\256\0
Flip Angle	180°	180°
Rows	512	512
Columns	408	512
Field of View (mm)	63*80	65*65

Table 1: List of MR imaging parameters.

Results

SpagoPix nanomaterial: SpagoPix consists of an organophosphosilane hydrogel with strongly chelated manganese (II) ions and a covalently attached PEG surface layer. It has a globular shape with an average hydrodynamic diameter 5 nm, as determined by both by GPC and DLS measurements. The zeta potential is essentially neutral. The longitudinal relaxivity (r_1) is 30 mM Mn $^{-1}$ s^{-1} (60 MHz) in both water and human blood plasma, which is significantly higher than the clinically used contrast agents [6].

Pharmacokinetics: The circulation time of SpagoPix in normal SD rats (n=3) was determined using Mn and Si as markers of nanomaterial payload and polymer matrix, respectively. Over the first 60 minutes after injection of SpagoPix, the plasma concentration of both Mn and Si declined by about 90%, with Mn dropping slightly faster Si. From 60 to 120 minutes both Mn and Si continued to fall but at a lower rate (Figure 1). A smaller study using mice with blood sampling at 5 and 15 was done to verify that there were no major species differences in circulation time. The results showed a similar profile (data not shown). Thus, SpagoPix nanoparticles are present in the circulation for more than one hour, defining the time frame in which extravasation to the tumor can occur.

MRI and CNR quantification: Between one and nine mammary tissue tumors were detected in all animals included in the study. The mean CNR of the tumors prior to administration of SpagoPix was 13.4 (+/- 4.52, n=24 tumors in 7 animals). Tumor contrast increased within 10 minutes after administration of SpagoPix (see Figure 2 for time resolved imaging series from one animal) and the mean CNR 30 min post administration of SpagoPix was 24.42 (+/- 7.90, n=29 tumors in 7 animals), see Figure 3. This corresponds to an 82 % increase in CNR. After 2-4 h, the mean CNR had further increased to 31.40 (+/- 11.17, n=31 tumors in 6 animals) corresponding to a 134 % CNR increase relative to the pre-SpagoPix imaging, see Figure 4. A boxplot and p-values are shown in Figure 5. In addition to an increased tumor CNR, the liver and gall bladder also exhibited increased MR signal intensities (Figure 6).

Bioanalysis of tumor and muscle tissues: After imaging, pieces of tumor, usually from beneath the forelimbs, and skeletal muscle from the hind limbs were excised and frozen. Tumor and skeletal muscle from one non-treated animal was included as a control. Since Mn is the component providing the MR contrast and Si is part of the nanomaterial matrix, the frozen tissues were digested and analyzed for content of these two elements. Tumors from MMTV-PyMT mice contained approximately 30 nmol Mn and 800 nmol Si per g tissue, which was 6- and 2-fold higher than in muscle tissue, respectively (Figure 7). Muscle tissues had approximately the same Mn and Si levels as tissues from non-injected animals.

Immunohistochemistry: The area of PEG (a coating constituent of SpagoPix) staining was large in tumors, whereas staining in muscle tissue was limited to scattered fibroblasts (Figure 8). The PEG staining area was larger at the later time points (2-4 h) compared to 30 minutes after injection as measured by image analysis (Figure 9). In contrast, muscles showed only a weak increase in PEG staining. The appearance of the staining in tumors was more focal at the early time point and more widespread throughout the tumor at the later time points.

Images for this section:

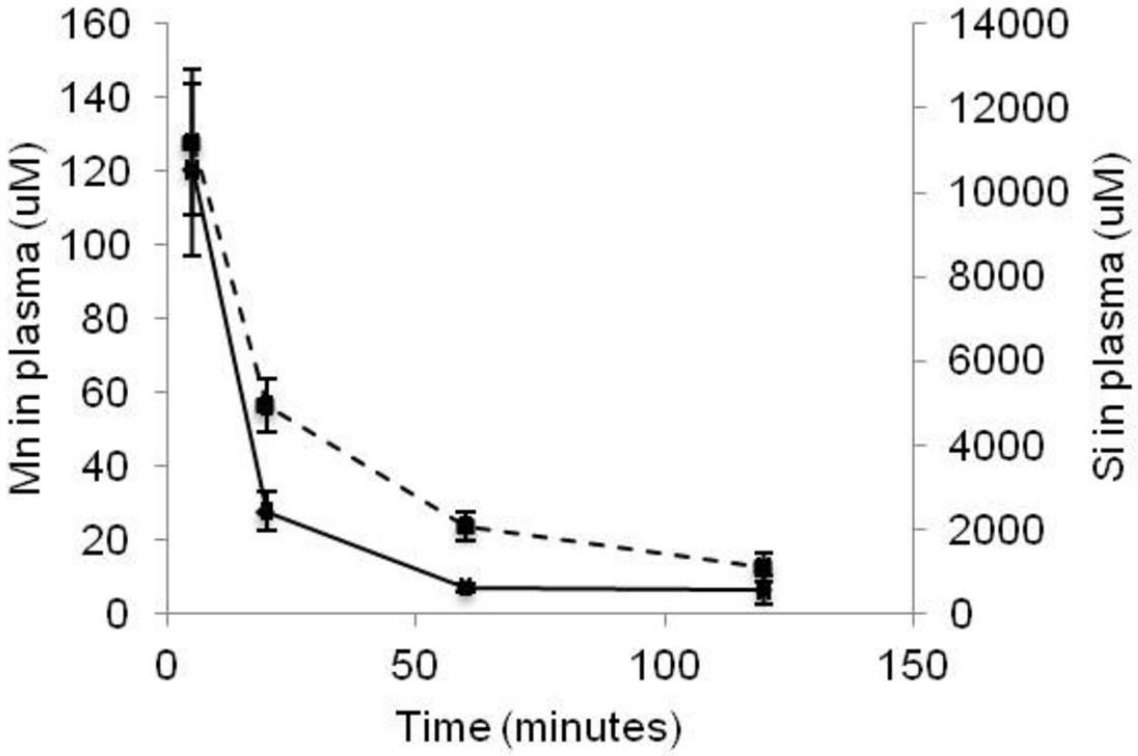

Fig. 1: Plasma concentrations of Mn (solid line) and Si (dotted line) in plasma of SD rats injected with SpagoPix.

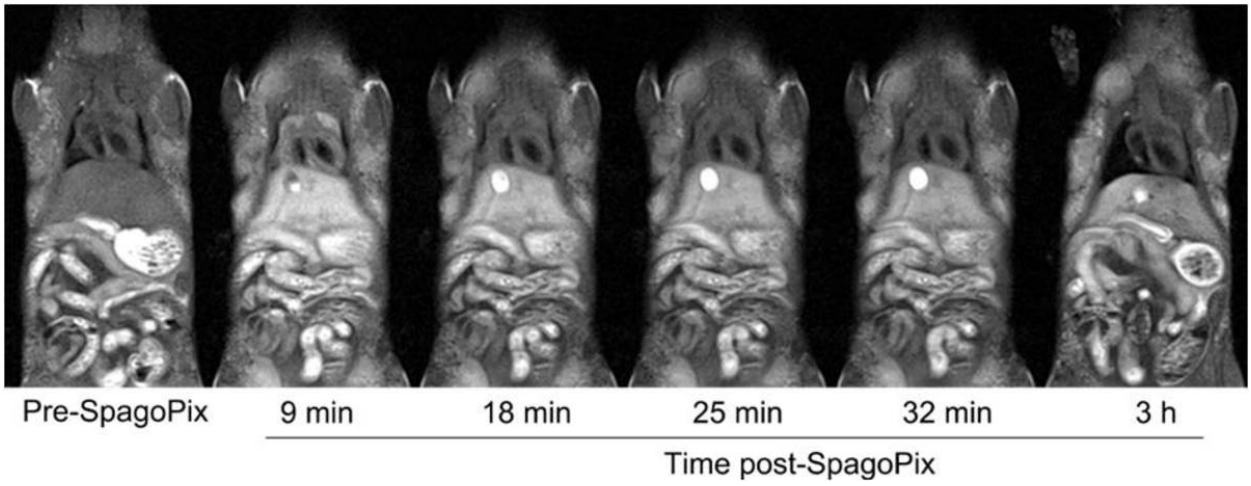

Fig. 2: MR images before injection of SpagoPix and 9 min to 3h post injection.

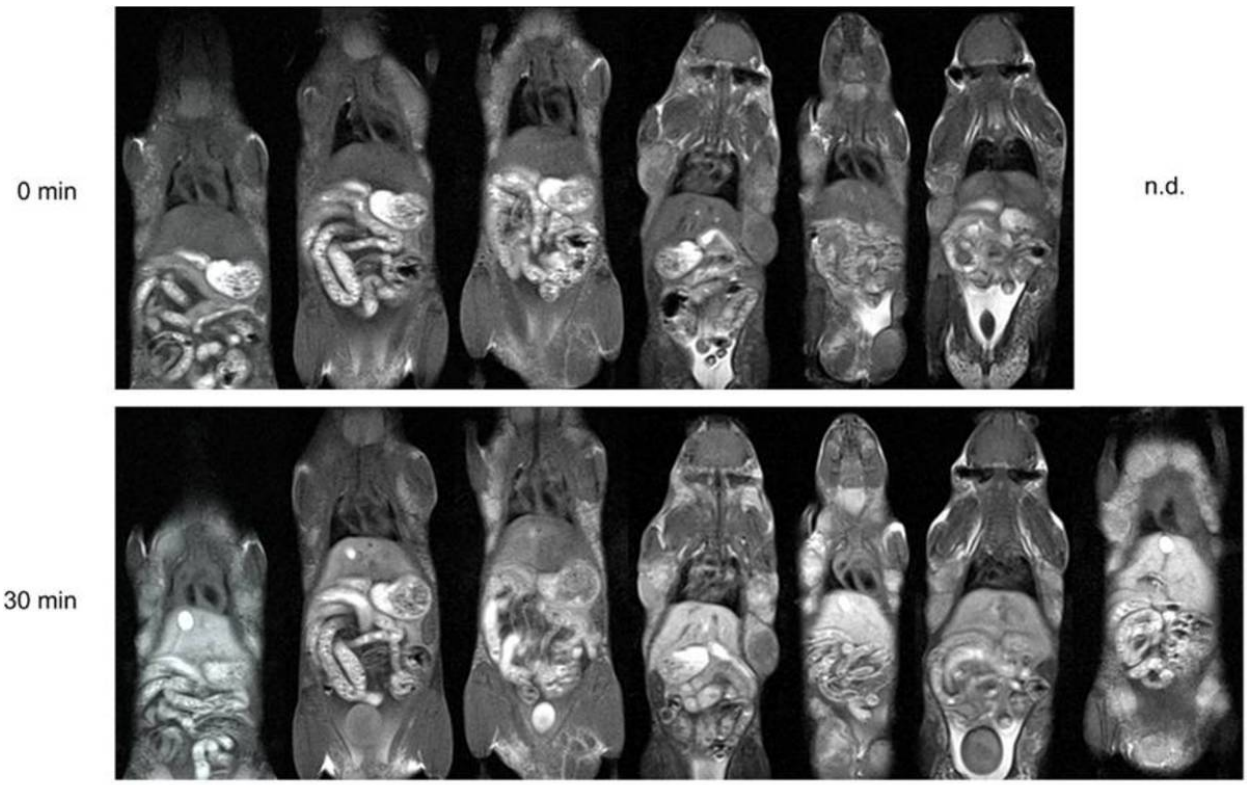

Fig. 3: MR images of 7 animals, before (top) and after 30 min after (bottom) administration of SpagoPix.

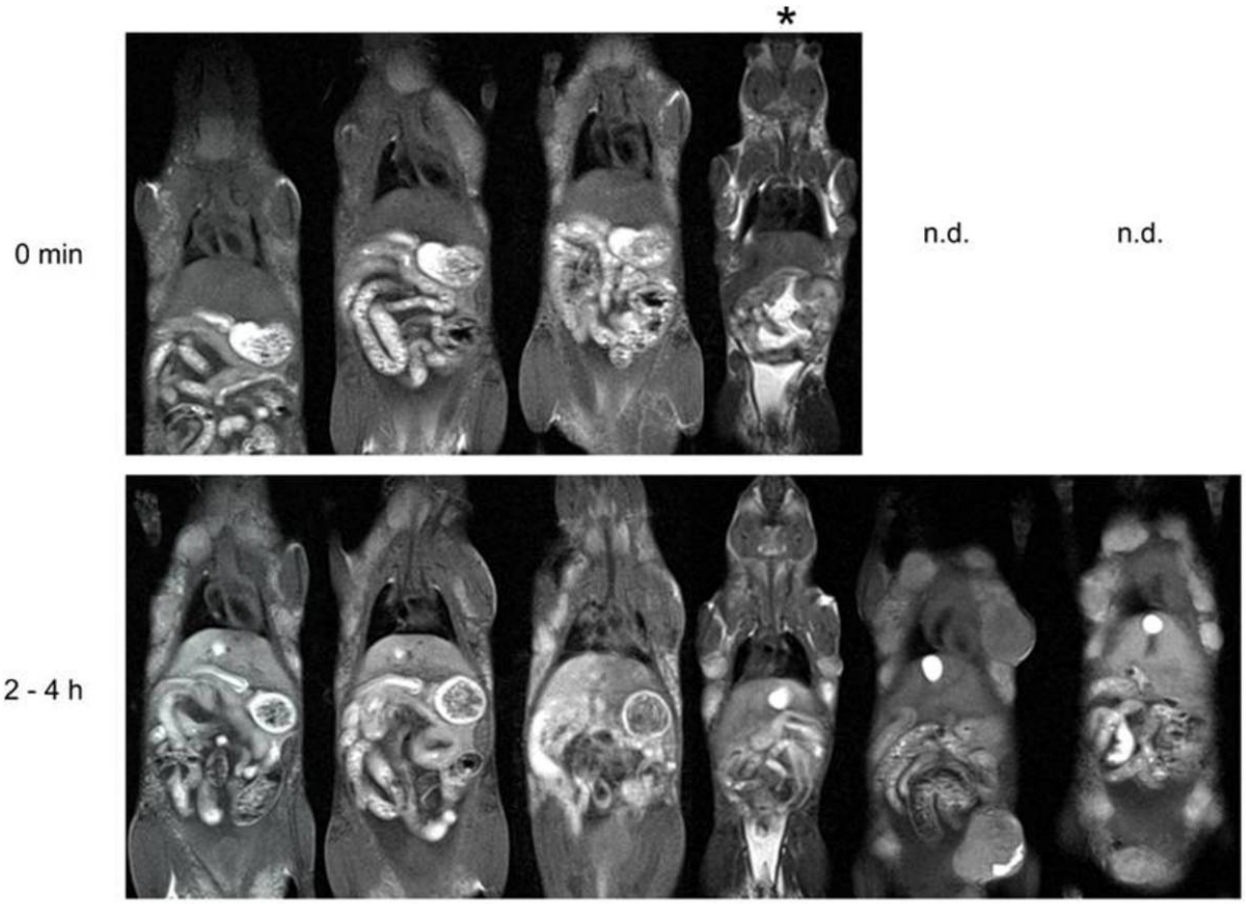

Fig. 4: MR images of 6 animals, before (top) and after 2 - 4 h after (bottom) administration of SpagoPix. Note that pre-injection imaging of the animal marked with an asterix (*) was done without fat saturation.

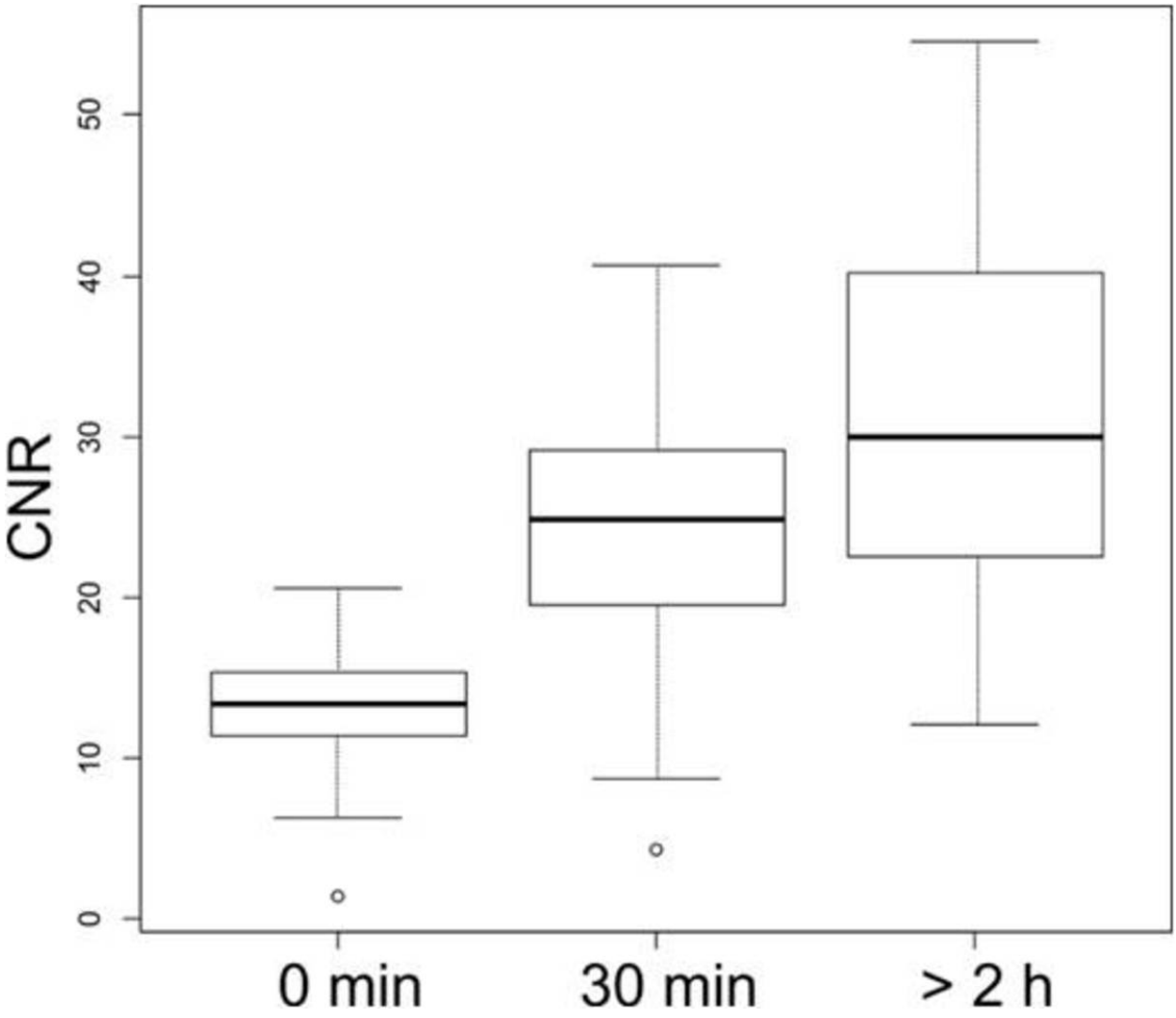

Fig. 5: Boxplot of CNR values for pooled tumors at T = 0 min (24 tumors in 7 animals), 30 min (29 tumors in 7 animals) and >2 h (31 tumors in 6 animals). P0-30min <0.0001, P0 min - >2 h <0.0001, P30 min - >2 h = 0.0074.

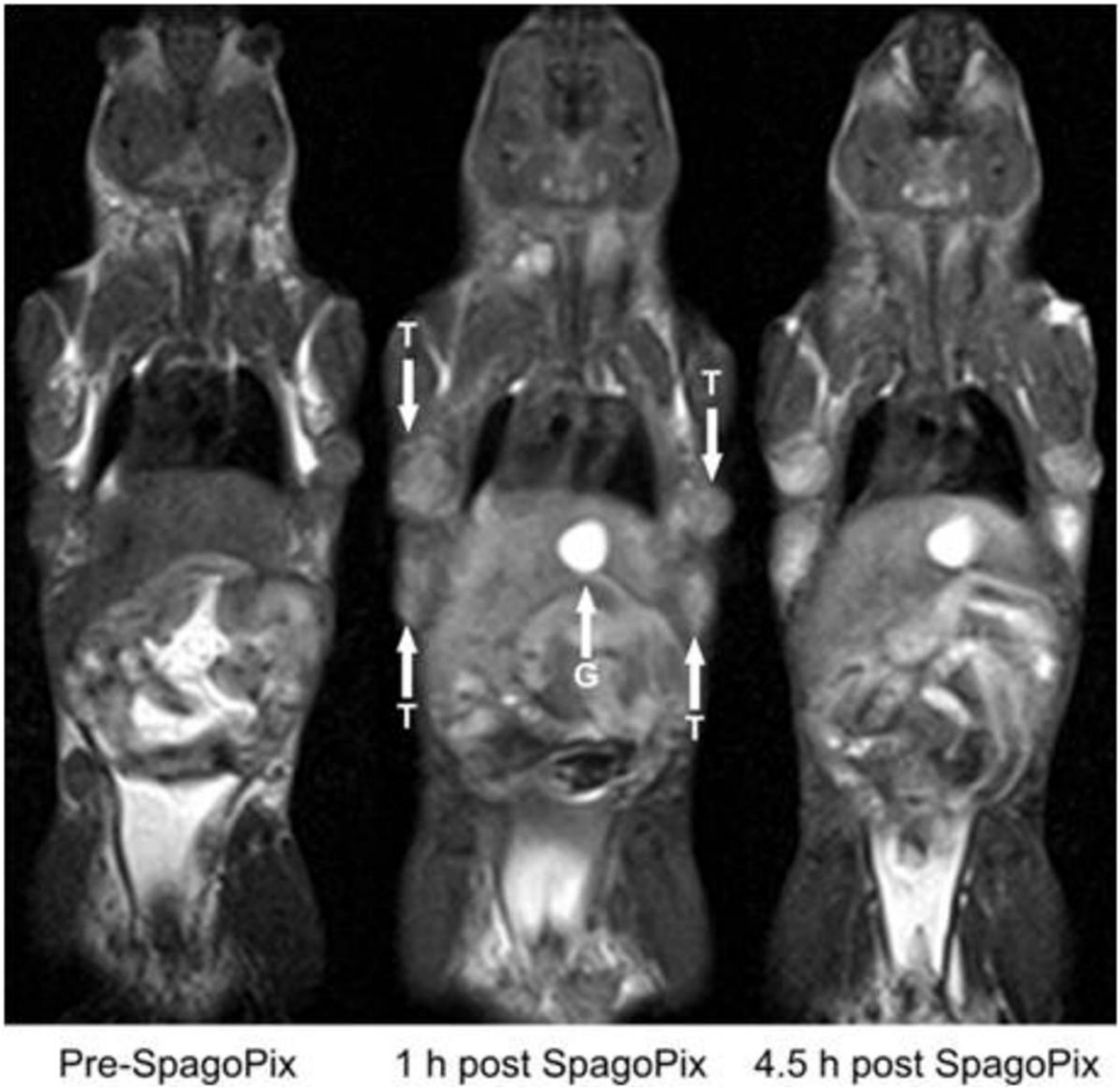

Fig. 6: MR images of pre-injection and 1 h and 4.5 h post injection, respectively, of SpagoPix. The 1 h image has tumors (T) and gall bladder (G) indicated with white arrows. Note that the pre-injection image is without applied fat saturation.

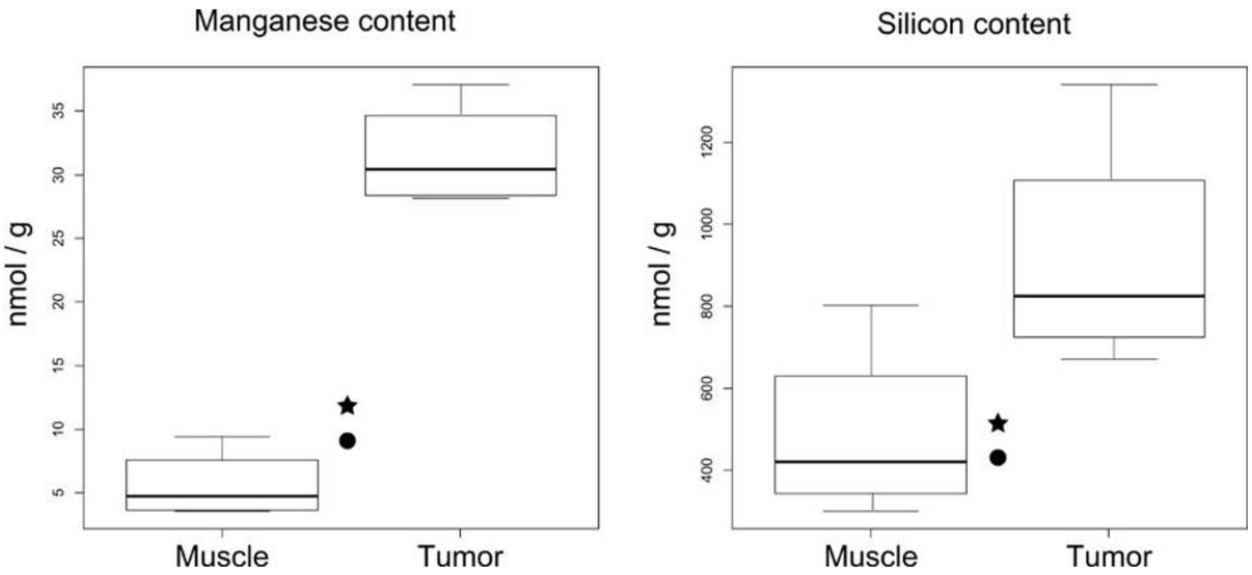

Fig. 7: Boxplots of manganese and silicon content in muscle and tumor tissue ~40 min to 4.5 h post injection of SpagoPix in MRI study 1 (n = 3 for ~40 min, n = 1 for 4 h). $p<0.001$ for manganese and $p>0.05$ for silicon. Background concentrations (n = 1) are indicated by stars (tumor) and circles (muscle).

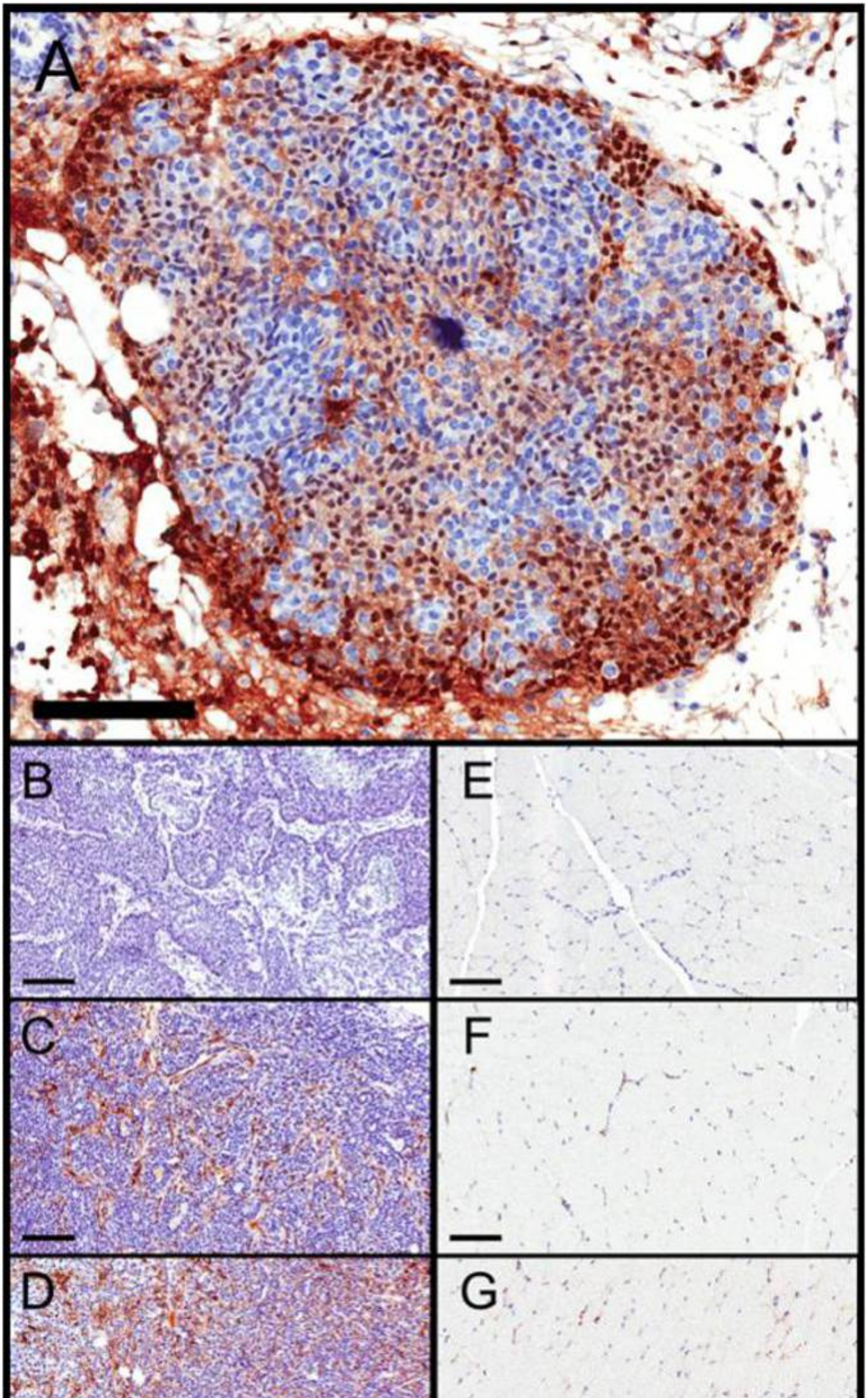
A
B
C
D
E
F
G

Fig. 8: Immunohistochemistry images of anti-PEG (brown) and hematoxylin counterstaining (blue). Tumor nodule two hours post-injection (A). Tumor (B, C, D) and muscle (E, F, G) tissue at pre-injection, 30 minutes and 2 hours post-injection, respectively. Bars indicate 100 µm.

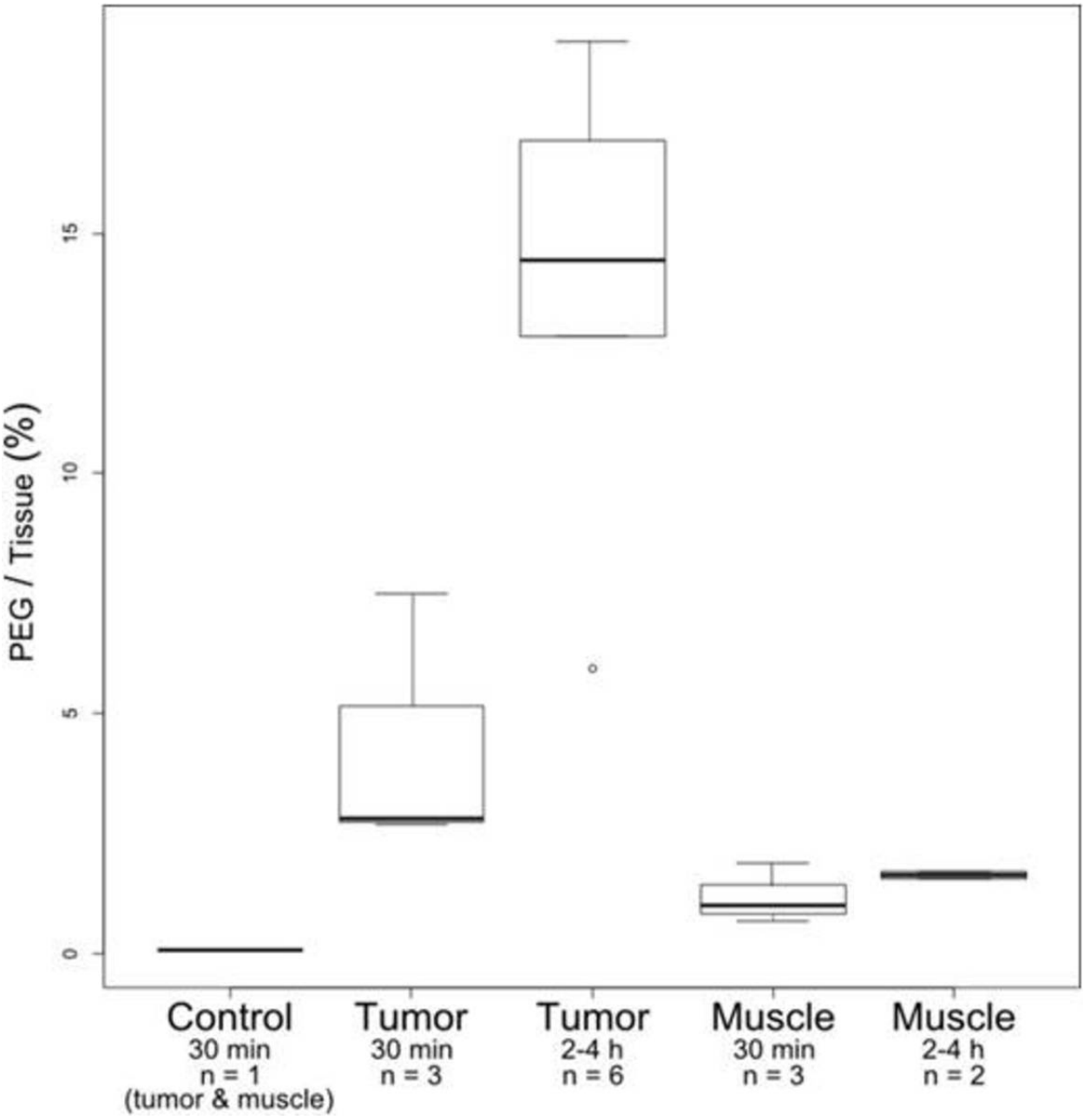

Fig. 9: PEG surface area in tumor and muscle at 30 minutes and 2-4 hours post-injection of SpagoPix. $p < 0.01$ for tumor at 2-4 h compared to muscle at 30 min and 2-4 h and compared to tumor at 30 min. The difference between tumor at 30 min and the muscle groups was not statistically significant.

Conclusion

Macromolecular CAs have been proposed as a way to selectively visualize tumors and tumor angiogenesis [7]. Ultra-small paramagnetic iron oxide (USPIO) particles (Feruglose, Amersham) of 30 nm size were shown both in preclinical models and in a clinical trial to be selectively taken up by malignant but not benign breast tissue lesions [8], [9]. This class of CAs (e.g. Resovist, Supravist) gives negative contrast and partly for that reason have found limited clinical utility, and then only as blood pool agents for magnetic resonance angiography (MRA).

To obtain blood pool agents with positive contrast, Gd-containing macromolecular CAs, including dendrimers and various copolymers [10] have been generated and shown promising results in preclinical models (e.g Gadomer-17 [11].

MS-325 is a small molecule with affinity for serum albumin, and it also has also shown promising preclinical data as a tumor imaging agent [12], but a relatively complex kinetic behavior has limited its use in clinical tumor diagnosis. It is however on the market indicated for aortoiliac occlusive disease under the trade name Ablavar™ (www.ablavar.com).

Due to the problem with NSF with Gd-containing CAs [13], manganese-containing macromolecular contrast agents have attracted more attention in recent years [3], [14]. Manganese has a more attractive safety profile than Gd, especially when complexed. Prolonged exposure to high doses, for instance shown for manganese mine workers, can cause neurotoxicity, but this is generally not considered an issue with intravenous injections of contrast agents [15]. Any polydisperse macromolecular agent will leave some long-lasting traces in the body. This would likely be unacceptable for Gd but Mn is an essential mineral nutrient and thus clearly more favorable from a safety perspective.

Our approach was to combine these two good features, tumor selectivity and safety profile, into a new type of CA - SpagoPix. This nanomaterial has an average hydrodynamic diameter of 5 nm and is neutral in charge. This size was chosen as a compromise between tumor selectivity and renal filtration, as it should give approximately 50% renal filtration [16].

The MR results showed that tumor to muscle contrast develops over a couple of hours. This is in line with a first phase where the nanomaterial enters the tumor and a second phase where the background is washed out leading to a gradual increase in CNR. The pharmacokinetic analysis and the MR results indicated that excess Mn is removed by the liver on the same time scale as the contrast develops. The nanomaterial matrix is to a large extent removed by renal filtration (data not shown).

The 82 % increase of contrast after 30 minutes and 134 % after 2-4 hours resulted in good tumor visualization, and importantly, all animals showed enhancement. The

implication of this is that also very small tumors should be detectable with high sensitivity. According to literature, the MMTV-PyMT model closely mimics human breast cancer at the histological and molecular levels [17]. In this model, the PyMT oncogene drives the development of well-differentiated, luminal-type adenomas that progress to metastatic, poorly-differentiated adenocarcinoma [18]. The benign adenomas are primarily found at an early age (4-8 weeks), while the animals studied here were 10-12 weeks old, and therefore the hypothesis of selective leakage into malignant lesions was not addressed.

The immunohistochemical analysis of PEG staining in tissues showed that the nanomaterial over time accumulated much more in tumor tissue than in muscle tissue, in a similar way as the tumor MR contrast developed. Interestingly, at the early time point the PEG staining was often localized near blood vessels, whereas after several hours it was more spread out, indicating that it had penetrated deeper into the tumor tissue. Only minor PEG staining was detected in muscle tissues demonstrating lack of vascular leakiness in this tissue. Further support for acccumulation of nanomaterial in the tumor came from the analysis of Mn and Si. Both elements increased after injection. The fact that no increase of Mn or Si was detected in muscle tissue again demonstrated the selectivity of the vascular leakage. Taken together, MR, IHC, and elemental analysis strongly support that SpagoPix selectively accumulates in tumors via the EPR effect and thus enhances their visibility.

In conclusion, the results presented herein, combined with those of Daldrup-Link et al., indicate that the Gd-free SpagoPix should allow characterization of lesions as benign or malignant with better specificity and no less sensitivity than current small molecule Gd CAs. Moreover, we have shown that SpagoPix allows for a more generous imaging time frame. Previous reports from preclinical studies have shown that the accumulation of macromolecular CAs is affected by angiogenesis inhibitiors [19], [20], implying that SpagoPix also has potential to be useful in monitoring such therapy.

Personal information

References

[1] A. R. Padhani, "Dynamic contrast-enhanced MRI in clinical oncology: current status and future directions," *J. Magn. Reson. Imaging JMRI*, vol. 16, no. 4, pp. 407-422, Oct. 2002.

[2] N. Houssami, S. Ciatto, P. Macaskill, S. J. Lord, R. M. Warren, J. M. Dixon, and L. Irwig, "Accuracy and surgical impact of magnetic resonance imaging in breast cancer staging: systematic review and meta-analysis in detection of multifocal and multicentric

cancer," *J. Clin. Oncol. Off. J. Am. Soc. Clin. Oncol.*, vol. 26, no. 19, pp. 3248-3258, Jul. 2008.

[3] D. Pan, A. H. Schmieder, S. A. Wickline, and G. M. Lanza, "Manganese-based MRI contrast agents: past, present and future," *Tetrahedron*, vol. 67, no. 44, pp. 8431-8444, Nov. 2011.

[4] H. Maeda and Y. Matsumura, "Tumoritropic and lymphotropic principles of macromolecular drugs," *Crit. Rev. Ther. Drug Carrier Syst.*, vol. 6, no. 3, pp. 193-210, 1989.

[5] O. Axelsson, R. M. Petoral Jr., F. Ek, and P. Lauritzson, "Novel Manganese Comprising Nanostructures," WO/2013/04162329-Mar-2013.

[6] M. Rohrer, H. Bauer, J. Mintorovitch, M. Requardt, and H.-J. Weinmann, "Comparison of magnetic properties of MRI contrast media solutions at different magnetic field strengths," *Invest. Radiol.*, vol. 40, no. 11, pp. 715-724, Nov. 2005.

[7] R. Brasch, C. Pham, D. Shames, T. Roberts, K. van Dijke, N. van Bruggen, J. Mann, S. Ostrowitzki, and O. Melnyk, "Assessing tumor angiogenesis using macromolecular MR imaging contrast media," *J. Magn. Reson. Imaging JMRI*, vol. 7, no. 1, pp. 68-74, Feb. 1997.

[8] H. Daldrup, D. M. Shames, M. Wendland, Y. Okuhata, T. M. Link, W. Rosenau, Y. Lu, and R. C. Brasch, "Correlation of dynamic contrast-enhanced MR imaging with histologic tumor grade: comparison of macromolecular and small-molecular contrast media," *AJR Am. J. Roentgenol.*, vol. 171, no. 4, pp. 941-949, Oct. 1998.

[9] H. E. Daldrup-Link, J. Rydland, T. H. Helbich, A. Bjørnerud, K. Turetschek, K. A. Kvistad, E. Kaindl, T. M. Link, K. Staudacher, D. Shames, R. C. Brasch, O. Haraldseth, and E. J. Rummeny, "Quantification of breast tumor microvascular permeability with feruglose-enhanced MR imaging: initial phase II multicenter trial," *Radiology*, vol. 229, no. 3, pp. 885-892, Dec. 2003.

[10] A. Bumb, M. W. Brechbiel, and P. Choyke, "Macromolecular and dendrimer-based magnetic resonance contrast agents," *Acta Radiol. Stockh. Swed. 1987*, vol. 51, no. 7, pp. 751-767, Sep. 2010.

[11] H. E. Daldrup-Link, D. M. Shames, M. Wendland, A. Mühler, A. Gossmann, W. Rosenau, and R. C. Brasch, "Comparison of Gadomer-17 and gadopentetate dimeglumine for differentiation of benign from malignant breast tumors with MR imaging," *Acad. Radiol.*, vol. 7, no. 11, pp. 934-944, Nov. 2000.

[12] K. Turetschek, E. Floyd, T. Helbich, T. P. Roberts, D. M. Shames, M. F. Wendland, W. O. Carter, and R. C. Brasch, "MRI assessment of microvascular characteristics in experimental breast tumors using a new blood pool contrast agent (MS-325) with

correlations to histopathology," *J. Magn. Reson. Imaging JMRI*, vol. 14, no. 3, pp. 237-242, Sep. 2001.

[13] M. A. Sieber, H. Pietsch, J. Walter, W. Haider, T. Frenzel, and H.-J. Weinmann, "A preclinical study to investigate the development of nephrogenic systemic fibrosis: a possible role for gadolinium-based contrast media," *Invest. Radiol.*, vol. 43, no. 1, pp. 65-75, Jan. 2008.

[14] M. Kueny-Stotz, A. Garofalo, and D. Felder-Flesch, "Manganese-Enhanced MRI Contrast Agents: From Small Chelates to Nanosized Hybrids," *Eur. J. Inorg. Chem.*, vol. 2012, no. 12, pp. 1987-2005, 2012.

[15] E. Chabanova, V. B. Logager, J. M. Moller, and H. S. Thomsen, "Manganese Based MR Contrast Agents: Formulation and Clinical Applications," *Open Drug Saf. J.*, vol. 2, pp. 29-38, Mar. 2011.

[16] B. Rippe, D. Venturoli, O. Simonsen, and J. de Arteaga, "Fluid and electrolyte transport across the peritoneal membrane during CAPD according to the three-pore model," *Perit. Dial. Int. J. Int. Soc. Perit. Dial.*, vol. 24, no. 1, pp. 10-27, Feb. 2004.

[17] E. Y. Lin, J. G. Jones, P. Li, L. Zhu, K. D. Whitney, W. J. Muller, and J. W. Pollard, "Progression to malignancy in the polyoma middle T oncoprotein mouse breast cancer model provides a reliable model for human diseases," *Am. J. Pathol.*, vol. 163, no. 5, pp. 2113-2126, Nov. 2003.

[18] C. T. Guy, R. D. Cardiff, and W. J. Muller, "Induction of mammary tumors by expression of polyomavirus middle T oncogene: a transgenic mouse model for metastatic disease," *Mol. Cell. Biol.*, vol. 12, no. 3, pp. 954-961, Mar. 1992.

[19] Q. G. de Lussanet, S. Langereis, R. G. H. Beets-Tan, M. H. P. van Genderen, A. W. Griffioen, J. M. A. van Engelshoven, and W. H. Backes, "Dynamic contrast-enhanced MR imaging kinetic parameters and molecular weight of dendritic contrast agents in tumor angiogenesis in mice," *Radiology*, vol. 235, no. 1, pp. 65-72, Apr. 2005.

[20] D. A. Beauregard, S. A. Hill, D. J. Chaplin, and K. M. Brindle, "The susceptibility of tumors to the antivascular drug combretastatin A4 phosphate correlates with vascular permeability," *Cancer Res.*, vol. 61, no. 18, pp. 6811-6815, Sep. 2001.